J. Fluid Mech. (2010), *vol.* 649, *pp.* 429–451. © Cambridge University Press 2010
doi:10.1017/S002211200999379X

Steady, unsteady and transient vortex-induced vibration predicted using controlled motion data

T. L. MORSE† AND C. H. K. WILLIAMSON

Sibley School of Mechanical and Aerospace Engineering, Cornell University, 144 Upson Hall, Ithaca, NY 14853, USA

(Received 15 March 2009; revised 29 November 2009; accepted 3 December 2009)

In this study, we represent transient and unsteady dynamics of a cylinder undergoing vortex-induced vibration, by employing measurements of the fluid forces for a body controlled to vibrate sinusoidally, transverse to a free stream. We generate very high-resolution contour plots of fluid force in the plane of normalized amplitude and wavelength of controlled oscillation. These contours have been used with an equation of motion to predict the *steady-state* response of an elastically mounted body. The principal motivation with the present study is to extend this approach to the case where a freely vibrating cylinder exhibits *transient* or *unsteady* vibration, through the use of a simple quasi-steady model. In the model, we use equations which define how the amplitude and frequency will change in time, although the instantaneous forces are taken to be those measured under steady-state conditions (the quasi-steady approximation), employing our high-resolution contour plots.

The resolution of our force contours has enabled us to define mode regime boundaries with precision, in the amplitude–wavelength plane. Across these mode boundaries, there are discontinuous changes in the fluid force measurements. Predictions of free vibration on either side of the boundaries yield distinct response branches. Using the quasi-steady model, we are able to characterize the nature of the transition which occurs between the upper and lower amplitude response branches. This regime of vibration is of practical significance as it represents conditions under which peak resonant response is found in these systems. For higher mass ratios ($m^* > 10$), our approach predicts that there will be an intermittent switching between branches, as the vortex-formation mode switches between the classical 2P mode and a '$2P_{OVERLAP}$' mode. Interestingly, for low mass ratios ($m^* \sim 1$), there exists a whole regime of normalized flow velocities, *where steady-state vibration cannot occur*. However, if one employs the quasi-steady model, we discover that the cylinder can indeed oscillate, but only with non-periodic fluctuations in amplitude and frequency. The character of the amplitude response from the model is close to what is found in free vibration experiments. For very low mass ratios ($m^* < 0.36$ in this study), this regime of unsteady vibration response will extend all the way to infinite normalized velocity.

1. Introduction

Vortex-induced vibration is important in many practical engineering applications. This phenomenon can lead to fatigue and failure of structures such as oil riser tubes, chimneys and bridges. There are a large number of fundamental studies on

† Email address for correspondence: tlm39@cornell.edu

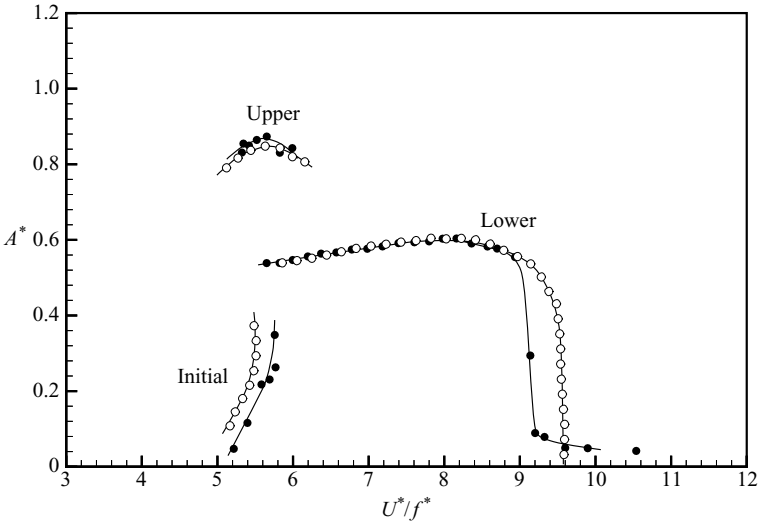

FIGURE 1. Comparison between steady-state predicted response and directly measured free vibration response ($m^* = 10.49$, $\zeta = 0$). The solid circle (●) denotes measured free vibration response from Govardhan & Williamson (2006), $Re = 4000$ at peak amplitude. The open circle (○) denotes predicted response from the present controlled vibration data, $Re = 4000$ throughout.

the subject, as well as several review articles, for example Sarpkaya (1979), Bearman (1984) and Parkinson (1989), and more recently Williamson & Govardhan (2004). Prior studies have investigated a selection of different flow configurations, including rigid cylinders moving with multiple degrees of freedom, pivoted cylinders or flexible cables. In this study, we choose to focus on the most conceptually simple case of vortex-induced vibration, that of an elastically mounted rigid cylinder constrained to move transverse to a flow. Such an arrangement is a paradigm in that it has been found to yield phenomena that are exhibited in the more complex configurations.

In many previous vortex-induced vibration studies, the focus has been on the amplitude and frequency response of the body (when it has reached a state of steady vibration) as a function of the incoming flow velocity. Khalak & Williamson (1999) showed that for a rigid cylinder with only transverse motion, and having a low combined mass-damping parameter, the amplitude of vibration exhibits three branches of response as the incoming flow velocity is increased: an initial branch, a high-amplitude upper branch and a lower branch; see figure 1. Over much of the response regime, the motion of the body is well represented by a sinusoidal function. However, in this study, we also focus on the behaviour of a cylinder as it exhibits *transient or unsteady dynamics*, in the transition regions between the different branches of response. These transition regions are significant, because the peak amplitude of vibration will often occur in an unsteady intermittent switching region between the upper and lower response branches, as found by Govardhan & Williamson (2006), in their recent study of peak amplitude response.

In the case of a controlled body, which is translated along a sinusoidal trajectory, Williamson & Roshko (1988) observed a set of different vortex-formation modes, existing within certain regimes in a plot of normalized amplitude and wavelength of the body motion. Among the vortex-formation modes, they found were a '2S' mode, representing two single vortices formed per cycle, a '2P' mode, meaning two

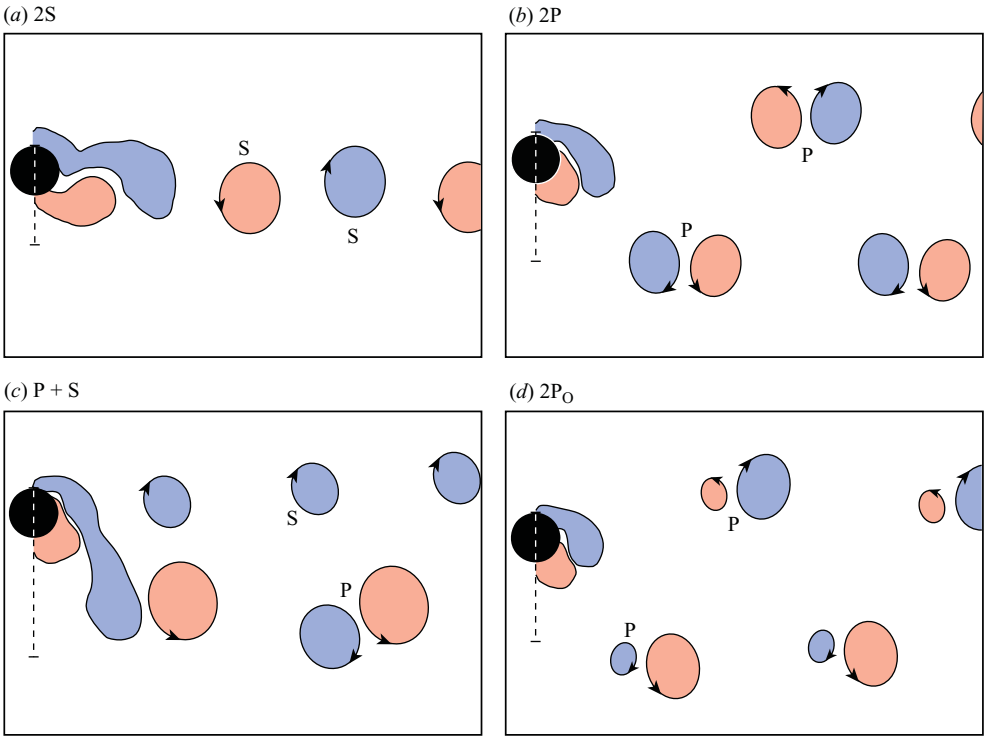

FIGURE 2. Representation of each of the main vortex-formation modes: {2S, 2P, P+S, 2P$_O$}. The 2P and 2P$_O$ modes show a similar pattern, with two vortices shed per cycle of vibration, except that in the 2P$_O$ case the secondary vortex is much weaker than the primary vortex.

pairs of vortices formed per cycle, and an asymmetric 'P+S' mode, comprising a pair of vortices and a single vortex in each cycle. Ongoren & Rockwell (1988) observed some comparable vortex-formation modes, in the case of a body oscillating in-line with the flow. The 2S, 2P and P+S modes are illustrated schematically in figure 2. The regimes of these modes within the amplitude–wavelength plane are shown in figure 3, in this case compiled using force measurements at a single Reynolds number value throughout the plane. This may be compared with the Williamson & Roshko map of regimes, compiled using flow visualization. In earlier studies (Morse & Williamson 2009*b*, 2009*c*) we identified a further new mode of vortex-formation, which is important because it is responsible for peak amplitudes of response in these flows, namely the 2P$_O$ mode, also illustrated in figure 2. This mode comprises two pairs of vortices in each cycle, but where the second vortex of each pair is distinctly smaller than the first vortex. It is defined as the '2P$_{OVERLAP}$' mode because its regime in the amplitude–wavelength plane overlaps other regimes as shown in figure 3.

Previous studies have observed different types of behaviours for the transition from the high-amplitude upper branch to the lower branch of response. Khalak & Williamson (1999) observed a range of normalized velocities where the amplitude would switch intermittently between an upper branch and lower branch level; these response branches are shown in figure 1. In other free vibration studies, rather than a jump from the upper to lower branch, the amplitude variation was found to be more continuous (e.g. Vikestad 1998; Bearman & Branković 2004; Hover,

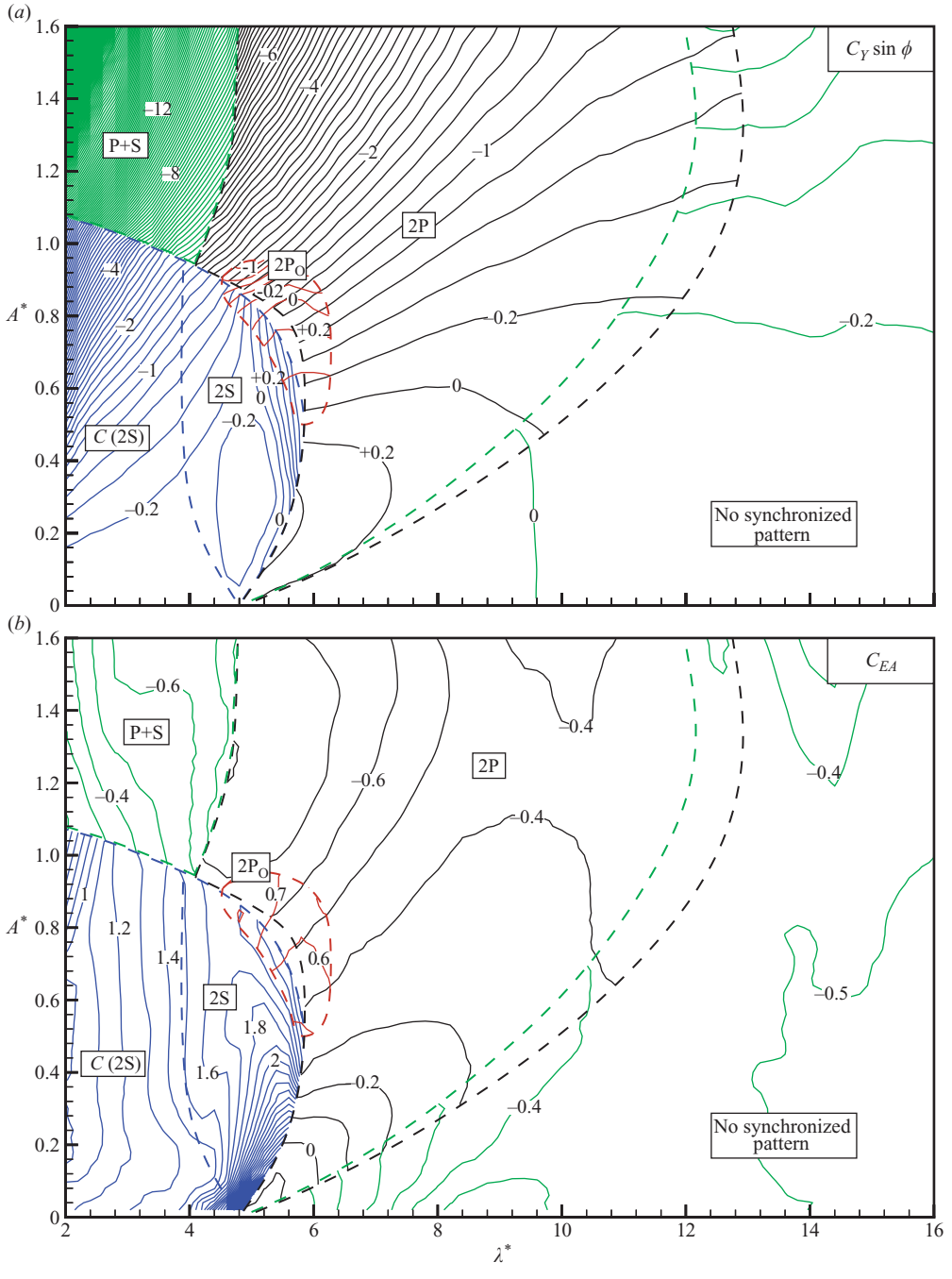

FIGURE 3. Contours of fluid forcing from controlled sinusoidal vibration at $Re = 4000$: (*a*) $C_Y \sin\phi$ with contour interval of 0.2 and (*b*) C_{EA} with contour interval of 0.1. Boundaries between modes are indicated by dashed lines; contours overlap in regions where multiple vortex shedding modes are possible.

Davis & Triantafyllou 2004). Note that, to some extent, interpretations of the amplitude response depend upon the algorithm used to determine amplitude from a data set.

Govardhan & Williamson (2000) characterized the switching behaviour for a system of moderate mass ratio ($m^* = 8.6$), and also for a system of very low mass ratio ($m^* = 1.2$), where $m^* =$ oscillating mass/mass of the fluid displaced. They found that for higher body mass ($m^* = 8.6$), the system would spend several cycles of vibration on one amplitude level, until there is an intermittent switch of both vortex mode and amplitude branch, causing the system to vibrate at a different clearly discernible amplitude level. However, for the $m^* = 1.2$ case, they observed rapid variations in amplitude (and frequency), which led them to suggest that a similar intermittent switching is present, but that it is possibly faster in this case. In the latter case, two distinct amplitude levels are not discernible. Therefore, in a response plot of maximum amplitude or mean amplitude, the transition from the upper branch to the lower branch would appear to be a continuous variation in amplitude.

Hover *et al.* (2004) also looked at the effect of mass ratio on the upper–lower transition region. They measured the correlation of fluid forces at opposite spanwise ends of a cylinder undergoing free vibration with $m^* = 3.0$ and showed that the correlation is quite high through most of the amplitude response plot, as one varies flow velocity, except in the region of the upper–lower branch transition. Employing hot-wire measurements along the span, they showed that the wake is quite three-dimensional in this transition region. Interestingly, they found that for a higher mass ratio ($m^* = 10$), the force correlation becomes high throughout the entire response, again suggesting a mass ratio effect on the nature of the upper–lower transition. Lucor, Foo & Karniadakis (2005) computed the flow for a cylinder undergoing transverse vibration with $m^* = 2.0$ and also found that near the transition from the upper branch to the lower branch there was a drop in the spanwise force correlation, and their computations showed that the wake primary vorticity was distinctly three-dimensional. On the basis of the three-dimensional nature of the wake in some cases, one might expect the measured force coefficient to depend on the cylinder aspect ratio. In this study, we have been careful to closely match the aspect ratio between free and controlled vibration (length/diameter is 10.0 for the controlled vibration cylinder and 8.3 for the free vibration cylinder). Such a close agreement may be more difficult with more disparate aspect ratios.

Our goal, in this study, is to gain further understanding of vortex-induced vibration when the amplitude or frequency varies in either a transient or an unsteady manner, and we shall study both the cylinder dynamics and the wake vortex dynamics. We are especially interested in the transition region between the upper and lower branches of response. Note that although this may appear to be a small regime (see e.g. figure 1), it can take up a large regime of normalized velocity (U^*), as shown below. Our approach will be to use controlled vibration force measurements, where the cylinder is prescribed to move with a sinusoidal motion, and we measure the fluid forces that act on the cylinder, over a wide range of normalized amplitude and frequency. Controlled vibration of a cylinder has been employed by a number of investigators, including Sarpkaya (1977), Staubli (1983), Gopalkrishnan (1993), Hover, Techet & Triantafyllou (1998) and Carberry, Sheridan & Rockwell (2005). Staubli, and Hover *et al.* have utilized their data sets to predict free vibration response plots.

In § 2, we describe the details of our experimental method which has allowed us to obtain very high resolution contour plots of fluid forcing in the plane of normalized amplitude and wavelength. In a previous paper (Morse & Williamson 2009*b*), we have used these contours to identify a set of regimes of vortex formation, which correspond well with the map of vortex-formation modes obtained by Williamson & Roshko (1988) from flow visualization. These contours were also used to predict *steady-state* behaviour of a freely vibrating cylinder. We include an example comparison between

prediction and direct free vibration measurement here in figure 1, where we find close agreement between steady-state solutions, using an equation of motion for a free vibration system described in §§ 3.1 and 3.2.

In this study, we extend our use of the finely resolved force contours, obtained for purely sinusoidal oscillations, to the case in which amplitude or frequency may vary in time. For this purpose, we develop a simple quasi-steady model in § 3.3. In the model, we use equations which define how the amplitude and frequency will change in time. However, for the instantaneous forces, we use those measured under steady-state conditions (the quasi-steady approximation), employing our high-resolution contour plots.

We use this simple model to predict transient behaviour, as the system approaches a final steady-state solution in § 4. In § 5, we apply the quasi-steady model to a system of low mass, and identify a *large regime of flow velocities for which the cylinder cannot vibrate in steady-state motion*; the model shows that it may only oscillate with an unsteady behaviour. We are thus able to characterize the nature of the upper branch to lower branch transition at high, moderate and low mass ratios using this approach, in close agreement with what is found from direct measurements of free vibration. This is followed by our conclusions in § 6.

2. Experimental details

These experiments are conducted in the Cornell-ONR Water Channel, which has a cross-section of 38.1×50.8 cm. The turbulence level in the test section of the water channel is less than 0.9 %. A cylinder of diameter 3.81 cm and length 38.1 cm is suspended vertically in the water channel and forced to oscillate transverse to the flow using a computer-controlled motor attached to a transverse lead screw. The controlled vibration system is automated and may be run unattended, allowing the acquisition of large sets of data. The flow speed is kept constant, to yield $Re = 4000$ throughout the data set. Following the study of Khalak & Williamson (1996), a fixed end plate is placed 2 mm below the bottom of the cylinder (but not in contact with the cylinder) to encourage two-dimensional vortex shedding. We measure fluid forces on the cylinder with a two-axis force balance utilizing LVDTs (linear variable differential transducers) over a wide range of normalized amplitude ($A^* = A/D =$ amplitude/diameter) and wavelength ($\lambda^* = \lambda/D =$ wavelength/diameter). It is convenient to use the parameter λ^* in this study, which is the normalized wavelength of the trajectory of the body relative to the fluid; $\lambda^* = U/fD$, where U is the free-stream velocity and f is the imposed frequency transverse to the flow. We vary A^* from 0.02 to 1.6, with a resolution of 0.02, and we vary λ^* from 2 to 16, with a resolution of 0.2, yielding a total of 5680 individual runs. For each run, the fluid force magnitude (F_1) and the phase angle (ϕ) at the fundamental (body oscillation) frequency are calculated using a Fourier series analysis. Relevant fluid forcing quantities, which will be introduced in the next section (for example, $C_Y \sin\phi$ and C_{EA}), are obtained using just the force component at the body oscillation frequency, which in general represents almost the entire force signal content. Because the prescribed motion is perfectly sinusoidal, the fundamental is the only frequency component of the fluid force which makes a net contribution to the energy transfer from fluid to body motion.

In order to determine vorticity using DPIV (digital particle image velocimetry), the flow is seeded with 14 μm silver coated glass spheres, which are illuminated by a sheet of laser light from a 50 mJ Nd:Yag pulsed laser. Pairs of particle images are acquired using a Jai CV-M2CL CCD camera (1600×1200 pixels) and analysed

using cross-correlation of sub-images. We use a two-step windowing process (with window shifting) to obtain particle displacements between image pairs. Vorticity fields calculated from the image pairs are phase averaged over approximately 10 cycles. More details on the force and PIV measurements may be found in Morse & Williamson (2009*b*).

3. Equations of motion and introduction of a quasi-steady model

In order to predict the dynamics of a freely vibrating cylinder from controlled vibration force measurements (both for steady-state and transient behaviours), we need to use the equation of motion for vortex-induced vibration in the transverse (y) direction (normal to the flow):

$$m\ddot{y} + c\dot{y} + ky = F(t), \tag{3.1}$$

where m is the oscillating mass, c is the structural damping, k is the spring constant and $F(t)$ is the fluid force in the transverse direction.

3.1. *Steady-state equations of motion for free vibration*

When the body has reached steady-state vibration and the motion is synchronized with the periodic vortex-formation mode, the force and displacement are generally well predicted by sinusoidal functions:

$$y(t) = A\sin\omega t, \tag{3.2}$$

$$F(t) = F_1\sin(\omega t + \phi), \tag{3.3}$$

where $\omega = 2\pi f$ and ϕ is the phase angle between the fluid force and the body displacement. The phase angle (ϕ) is an important quantity as it determines the direction of energy transfer between the fluid and the body motion; it must be between 0 and 180° for the fluid excitation to be positive, and hence for free vibration to occur. Our selected set of non-dimensional parameters in this problem is presented in table 1. In particular, the principal parameters defining the body motion are the normalized amplitude (A^*) and the frequency ratio (f^*) in a flow of normalized velocity U^*.

If we substitute (3.2) and (3.3) into the equation of motion (3.1), we can obtain the 'amplitude equation':

$$A^* = \frac{1}{4\pi^3}\frac{C_Y\sin\phi}{(m^* + C_A)\,\zeta}\left(\frac{U^*}{f^*}\right)^2 f^*, \tag{3.4}$$

which includes the force coefficient in phase with the body velocity ($C_Y\sin\phi$), equivalent to a normalized energy transferred from the fluid to the cylinder, which is also called the fluid excitation. We may similarly obtain the 'frequency equation':

$$f^* = \sqrt{\frac{m^* + C_A}{m^* + C_{EA}}}, \tag{3.5}$$

where C_A is the potential flow added-mass coefficient ($C_A = 1.0$ for a circular cylinder), and C_{EA} is an 'effective' added-mass coefficient that includes an apparent mass effect due to the total transverse fluid force in phase with the body acceleration ($C_Y\cos\phi$):

$$C_{EA} = \frac{1}{2\pi^3}\frac{C_Y\cos\phi}{A^*}\left(\frac{U^*}{f^*}\right)^2. \tag{3.6}$$

Mass ratio	m^*	$\dfrac{m}{\pi\rho D^2 L/4}$
Damping ratio	ζ	$\dfrac{c}{2\sqrt{k(m+m_A)}}$
Normalized velocity	U^*	$\dfrac{U}{f_N D}$
Normalized wavelength	λ^*	$\dfrac{\lambda}{D} = \dfrac{U}{fD}$
Normalized amplitude	A^*	$\dfrac{A}{D}$
Frequency ratio	f^*	$\dfrac{f}{f_N}$
Transverse force coefficient	C_Y	$\dfrac{F_Y}{\frac{1}{2}\rho U^2 DL}$
Reynolds number	Re	$\dfrac{\rho U D}{\mu}$

TABLE 1. Non-dimensional groups. In the above groups, U is the free-stream velocity, λ is the oscillation wavelength, f is the oscillation frequency, f_N is the natural frequency in water, D is the cylinder diameter, L is the submerged cylinder length, ν is the fluid kinematic viscosity, ρ is the fluid density and F_Y is the transverse fluid force. The added mass, m_A, is given by $m_A = C_A m_d$, where m_d is the displaced fluid mass and C_A is the potential added-mass coefficient ($C_A = 1.0$ for a circular cylinder).

The amplitude and frequency equations derived above must hold if the cylinder is oscillating with steady-state (sinusoidal) vibration. Over much of a free vibration response plot, as in figure 1, the body motion and the fluid forcing are quite sinusoidal and the above equations (3.4), (3.5) and (3.6) are sufficient to accurately predict the amplitude and frequency of motion. A principal interest in this study is to extend free vibration prediction to cases in which the amplitude and frequency vary. We shall see that such conditions can, for a low mass ratio, persist for large portions of a response plot. In order to make such predictions, we employ a quasi-steady assumption described in § 3.3.

3.2. *Contours of fluid forcing*

From our high-resolution controlled vibration force measurements, in figure 3 we present contour plots of the fluid forcing quantities $C_Y \sin\phi$ and C_{EA}, in a plot of normalized amplitude (A^*) and normalized wavelength (λ^*) which represent the sinusoidal trajectory for the cylinder relative to the fluid. The normalized wavelength is equivalent to the flow velocity normalized by the oscillation frequency ($\lambda^* = U^*/f^* = U/fD$). The fluid excitation plot showing contours of $C_Y \sin\phi$ in figure 3(a) was first presented by Morse & Williamson (2009b).

In certain regions of the parameter space, we find jumps in the character of the fluid forcing, and thus are able to identify boundaries separating different fluid forcing regimes, which correspond to boundaries separating different vortex-shedding modes in the Williamson & Roshko (1988) map of regimes. Vorticity measurements confirm the modes of vortex formation in each regime, including the 2S, 2P and P+S modes,

introduced in § 1, as well as a regime where the vortex formation is not synchronized with the cylinder oscillation.

We also identify regions where two vortex-formation regimes overlap, as may be seen in the contours of figure 3. In these regions, the wake may switch intermittently between two distinct modes even as the cylinder is vibrating with constant amplitude and frequency, as first shown by Morse & Williamson (2009*b*). In the principal overlap region, we identify a $2P_O$' (or $2P_{OVERLAP}$) mode of vortex formation where two pairs of vortices are shed per cycle of oscillation (similar to the classical 2P mode) but where the secondary vortex is much weaker than the primary vortex in each pair, as described briefly in § 1 (see figure 2*d*). The existence of an overlapping mode is significant because it is associated with the maximum amplitude where positive excitation occurs. It will thus be the mode yielding the peak resonant amplitude in free vibration. We shall also see that the overlap of the $2P_O$ mode with the 2S and 2P regimes leads to some interesting unsteady body dynamics, which are discussed in §§ 4 and 5. A comprehensive characterization of the different changes was found as one crosses the regime boundaries, shown in figure 3, including time traces and spectra for the different forcing regimes, may be found in Morse & Williamson (2009*b*).

From the force contours in figure 3, we can predict the steady-state (sinusoidal) response (amplitude, A^*, and frequency, f^*) of a freely vibrating cylinder for a given set of system parameters $\{m^*, \zeta, U^*\}$. We simply find the point (or points) in the amplitude–wavelength plane where both the amplitude equation (3.4) and frequency equation (3.5) are satisfied. By varying the normalized velocity (U^*), we can build up an entire response plot. As an introduction to the present results, we show in figure 1 that the steady-state response of a freely vibrating cylinder can be accurately predicted (taken from Morse & Williamson 2009*c*). The initial branch will have a 2S vortex-formation mode, the upper branch a $2P_O$ mode and the lower branch a 2P mode.

3.3. *Quasi-steady model for free vibration response*

In this work, we would like to extend our prediction of freely vibrating cylinder dynamics to transient or unsteady behaviour. To do this, we will need to introduce a quasi-steady assumption. Specifically, we assume that as the amplitude or frequency of oscillation is varying, the instantaneous fluid forcing (magnitude and phase) is given by our controlled vibration force contours for purely sinusoidal motion at the instantaneous value of the amplitude and frequency. Naturally, we expect that this assumption will be more accurate for slower variations in amplitude or frequency.

Our goal is to implement this quasi-steady assumption in a model that is both simple and useful. Therefore, we will not attempt to determine the cylinder dynamics in terms of $y(t)$ but rather we will assume that the motion takes on a sinusoidal form, but with varying amplitude and frequency. Therefore, we will be solving for $A^*(\tau)$ and $f^*(\tau)$, where $\tau = t/T$ (or time/period) of oscillation, and the solution will be advanced in fractions of the oscillation period. We know that as the system approaches a steady-state solution (constant amplitude and frequency), the model should reduce to the steady-state amplitude and frequency equations determined above, (3.4) and (3.5).

We use the form of the amplitude equation to define an 'effective damping', ζ_{eff}, which includes the structural damping as well as the effect of the fluid excitation, $(C_Y \sin\phi)$, as follows:

$$\zeta_{eff} = \zeta - \frac{C_Y \sin\phi}{4\pi^3 (m^* + C_A) A^*} \left(\frac{U^*}{f^*}\right)^2 f^*. \tag{3.7}$$

Similarly, we define an 'effective mass', m^*_{eff}, which includes the structural mass as well as an effective added mass due to the fluid forcing in phase with acceleration ($C_Y \cos\phi$) as follows:

$$m^*_{eff} = m^* + \frac{1}{2\pi^3}\frac{C_Y \cos\phi}{A^*}\left(\frac{U^*}{f^*}\right)^2 = m^* + C_{EA}. \tag{3.8}$$

We then assume that the system behaves like a simple spring-mass-damper system except that the mass (m^*_{eff}) and the damping (ζ_{eff}) can dynamically vary depending on the instantaneous amplitude or frequency. The effective damping will determine if the amplitude increases or decreases as follows:

$$\frac{\mathrm{d}A^*}{\mathrm{d}\tau} = \left(-2\pi\zeta_{eff} f^*\right) A^*, \tag{3.9}$$

which is the well-known equation for amplitude decay in damped harmonic vibration. The effective mass will affect the frequency of oscillation as follows:

$$f = \frac{1}{2\pi}\sqrt{\frac{k}{m_{eff}}}. \tag{3.10}$$

We normalize this frequency by the natural frequency in still water (f_N) to yield

$$f^* = \sqrt{\frac{m^* + C_A}{m^*_{eff}}}. \tag{3.11}$$

To implement the model, we first need to define the system parameters $\{m^*, \zeta, U^*\}$ and initial values for A^* and f^*. Then we look up the values of ($C_Y \sin\phi$) and C_{EA} from the contours in figure 3. At this point, we use (3.9) to determine the change in amplitude over one time step, and we then advance A^*. Similarly, we use (3.11) to find the new value of frequency f^* at the end of the time step. We let the time step, $\Delta\tau$, vary so that the amplitude or frequency does not change by too great an amount (more than typically 5 %) in one iteration.

A complication with implementing the model is that at some points in the amplitude–wavelength plane there are two possibilities for the fluid forcing, as two modes of vortex formation are possible, shown as overlapping contours in figure 3. Of course, this overlap phenomenon (between the 2S and $2P_O$ modes and between the $2P_O$ and 2P modes) is what leads to some of the interesting behaviour observed in vortex-induced vibration systems, such as the intermittent switching between the upper and lower branches of response, as we explain in § 4.2. We will therefore handle the overlap regions in two different ways, as described in the following sections.

4. Transient behaviour for moderate and high mass ratio systems

For a vortex-induced vibration system, the equilibrium solution (i.e. the amplitude and frequency for steady-state vibration) will be the intersection of the curves along which the amplitude equation (3.4) is satisfied, and the curve along which the frequency equation (3.5) is satisfied. The curves will generally not be continuous, showing jumps when the vortex-formation mode changes. In this section, we use the quasi-steady model to determine how the equilibrium solutions are approached.

4.1. *Approaching a lower branch equilibrium*

We begin with a simple starting case: a system having moderate mass ratio, $m^* = 10.0$, and very low damping, $\zeta = 0.001$, at normalized velocity, $U^* = 8.0$. For this case, there

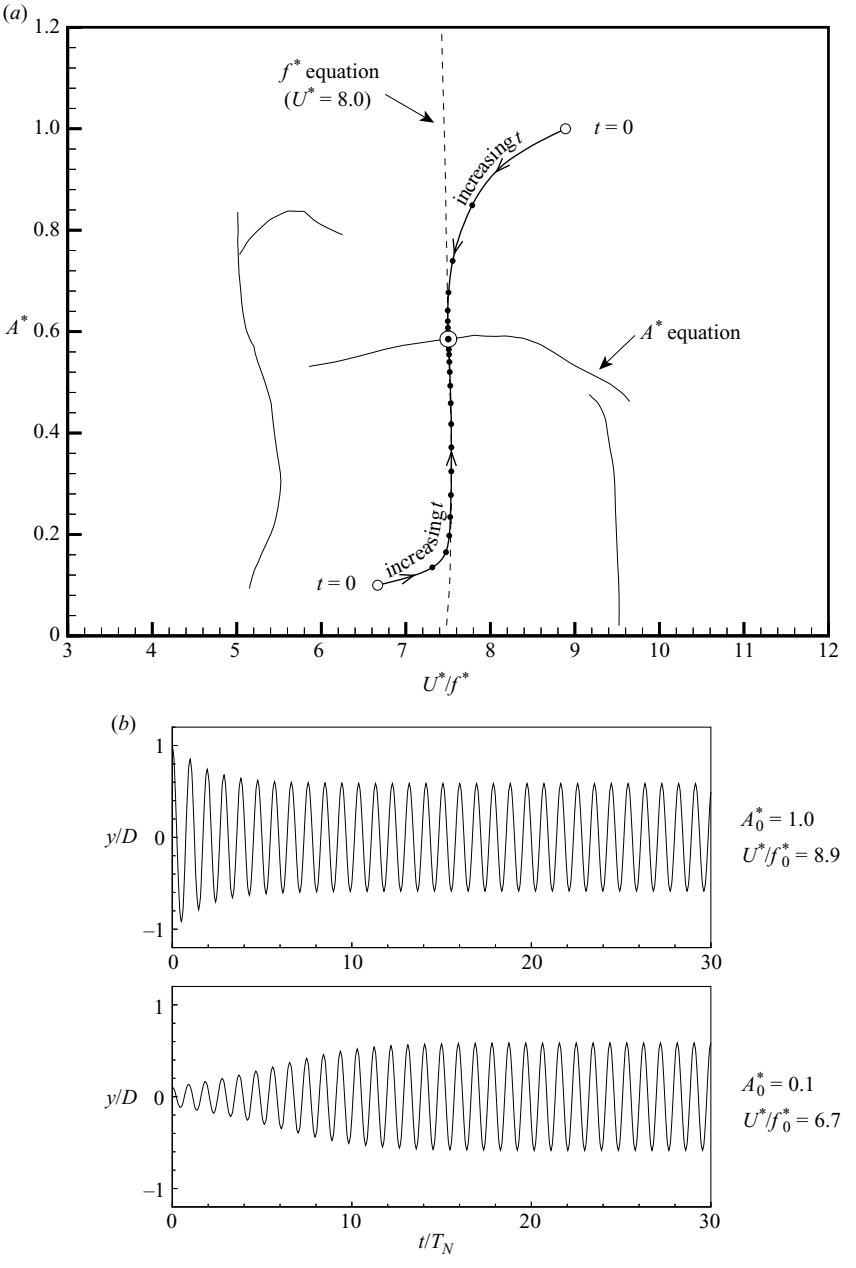

FIGURE 4. Prediction of transient behaviour for an equilibrium solution in the lower branch, $m^* = 10$, $\zeta = 0.001$, $U^* = 8.0$. In (a) we show how the equilibrium solution ⊙ is approached for arbitrary initial conditions ○. The solid circle (●) indicates location after each cycle of oscillation. In (b) we show time traces for the two initial conditions investigated.

is an equilibrium solution in the lower branch of a free vibration response, as shown by the bull's eye in figure 4(a). We choose to look for solutions in the (A^*, U^*/f^*) space, because that is the parameter space for our controlled vibration contours (note that $\lambda^* = U^*/f^*$). This is equivalent to the (A^*, f^*) space because we are fixing the value of the normalized velocity U^*.

Employing our quasi-steady model, we give the system arbitrary initial conditions and observe how the system approaches the equilibrium solution. As can be seen in figure 4(*b*), for this example, it happens to take longer for a low-amplitude initial condition to reach the equilibrium solution than for a high-amplitude initial condition. This is because the contour levels of fluid excitation ($C_Y \sin\phi$) are closer together for the higher amplitude approach to the equilibrium solution (there is a steeper gradient of excitation versus amplitude). In summary, the technique appears to work well in such examples.

4.2. *Intermittent switching between upper and lower branch equilibria*

One of our main goals in developing our quasi-steady model is to predict the cylinder dynamics in the upper to lower branch transition regions of a free vibration response. In figure 5(*a*), a system with $U^* = 6.3$ will have two equilibrium solutions, depending on the mode of vortex formation. For the $2P_O$ mode, the equilibrium solution will lie in the upper branch; for the pure 2P mode, the equilibrium solution will lie in the lower branch.

In order to observe the switching behaviour, we run the quasi-steady model twice. In the first case, we give the system the initial conditions corresponding to the upper branch equilibrium (see bull's eye for the $2P_O$ mode in figure 5*a*), but we use the force contours for the 2P mode at these same initial conditions. The 2P mode yields negative fluid excitation at the higher upper branch amplitude, so it cannot sustain free vibration; the amplitude must drop to the lower branch level, where the fluid excitation is positive. We then perform the reverse, selecting the lower branch initial conditions, but using the $2P_O$ mode forces at those same conditions, and observe how the amplitude increases to the upper branch. For a freely vibrating cylinder, we expect that the switch in vortex-formation mode will happen randomly. Here we arbitrarily decide when the vortex-formation mode switches and build up an intermittent switching time trace, shown in figure 5(*b*), which we compare with an actual intermittent switching time trace from Govardhan & Williamson (2000), in figure 5(*c*). In choosing moments in time where we switch modes, we are guided by the experimental data in figure 5(*c*) in this particular case.

We are interested in the number of cycles required for the amplitude to make a transition. We see that a typical experimental drop in amplitude from the upper branch to the lower branch is well represented by our quasi-steady model predictions. However, the experimental rise in amplitude from the lower branch to the upper branch appears to take a few cycles longer than our predictions. We attribute this to the stipulation in our model that the vortex-formation mode changes instantaneously. For a real system, there may be several cycles of oscillation over which the vortex-formation mode changes from 2P to $2P_O$, before the system can start to more rapidly increase amplitude.

We can make an estimate of how fast the vortex-formation mode switches, by observing time traces of the phase angle from our controlled vibration force measurements, in figure 6. The 2P mode will have a phase angle of around 180° while the $2P_O$ mode will have a phase angle of around 0° (see Morse & Williamson 2009*b* for a detailed description of the force characteristics for each mode. For lower amplitudes, the switch in phase takes several cycles of vibration, whereas at higher amplitudes, the switch occurs nearly instantaneously, as may be observed in figure 6. Therefore, at low amplitudes, when the vortex-formation mode switches from 2P to $2P_O$, we expect that several additional cycles of oscillation are required for the vortex-formation mode to change. Our model does not include such an effect.

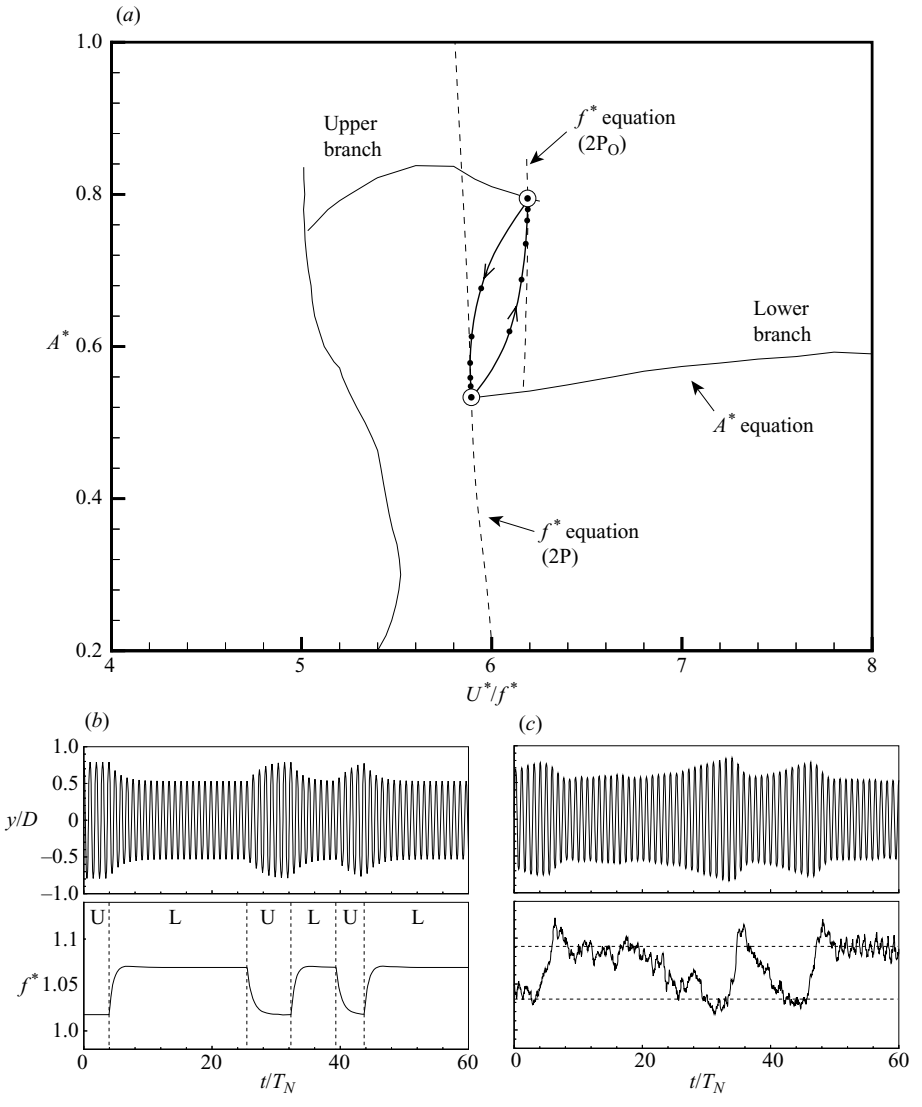

FIGURE 5. Prediction of intermittent switching transient behaviour, $m^* = 10$, $\zeta = 0.001$, $U^* = 6.3$. In (*a*) the quasi-steady model to determine the dynamics of the cylinder as it moves between an equilibrium point ⊙ in the 2P and $2P_O$ regimes (the lower and upper branches). In (*b*) we show a predicted time trace, which we compare with an actual free vibration intermittent switching time trace at $m^* = 8.63$ from Govardhan & Williamson (2000) in (*c*).

5. Unsteady behaviour for very low mass ratio systems

We now turn to another case in which the quasi-steady model proves to be quite revealing: that of a very low mass ratio system. In § 3, we showed how we may predict the response of a freely vibrating cylinder at moderate mass ratio, $m^* = 10$. One of the well-known results from previous vortex-induced vibration studies is that, as the mass ratio decreases, there is a widening of the range of normalized velocity (U^*) over which vibration occurs (an effect observed originally by Ramberg & Griffin 1981). We are in a position to predict this result employing our controlled vibration data.

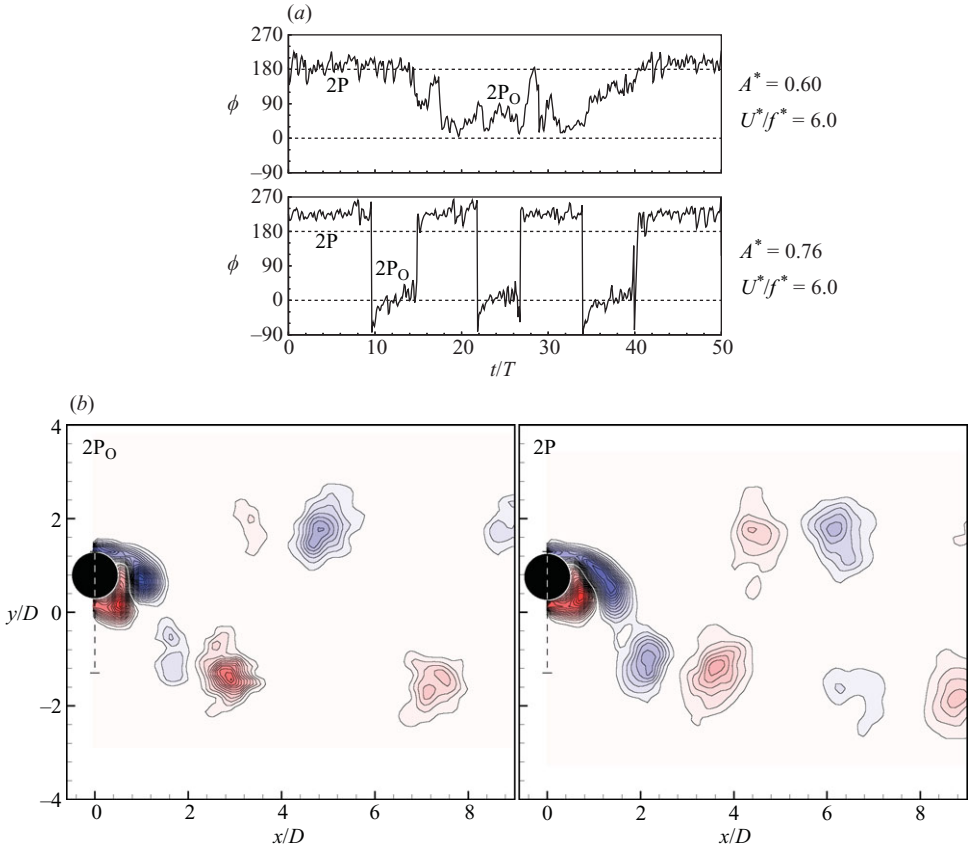

FIGURE 6. Phase-switching and vortex-formation modes in the 2P–2P$_O$ overlap regimes. (*a*) The phase between cylinder motion and fluid force, showing more rapid transitions between modes for the higher amplitude case than for the lower amplitude case. (*b*) Vorticity fields for the 2P and 2P$_O$ vortex-formation modes, both obtained at $A^* = 0.8$, $U^*/f^* = 5.6$. Contour levels shown are $\omega D/U = \pm 0.4, \pm 0.8, \pm 1.2, \ldots$.

5.1. *The effect of reducing mass ratio on the upper branch to lower branch transition*

At moderate mass ratio, $m^* = 15$ (and zero damping), we use our controlled vibration data to predict the steady-state response of a free vibration system. The regime of response extends up to $U^* \approx 10$, as shown in figure 7(*a*). Also, there is a small range of normalized velocity for which two steady-state solutions exist (thus two possible amplitudes of vibration) in the region between the upper and lower response branches close to $U^* = 6$. In § 4.2, we indicated how this is associated with intermittent switching between the branches. As we decrease mass ratio, we find a certain special value ($m^* = 7.7$) where the upper and lower branches no longer overlap, and there is one value of amplitude for each value of normalized velocity as shown in figure 7(*b*).

As we decrease mass ratio even further to $m^* = 1.0$ (still with zero damping), we find a further widening of the regime of velocity (U^*) for which vibration occurs as shown in figure 8(*a*). However, we encounter a seemingly intractable problem: we find large regimes of velocity (in this case, $U^* = 7$ to 11 in figure 8) where there is no steady-state solution to the equations of motion, i.e. *no points for which both the amplitude and frequency equations are satisfied*. This would seem to suggest that

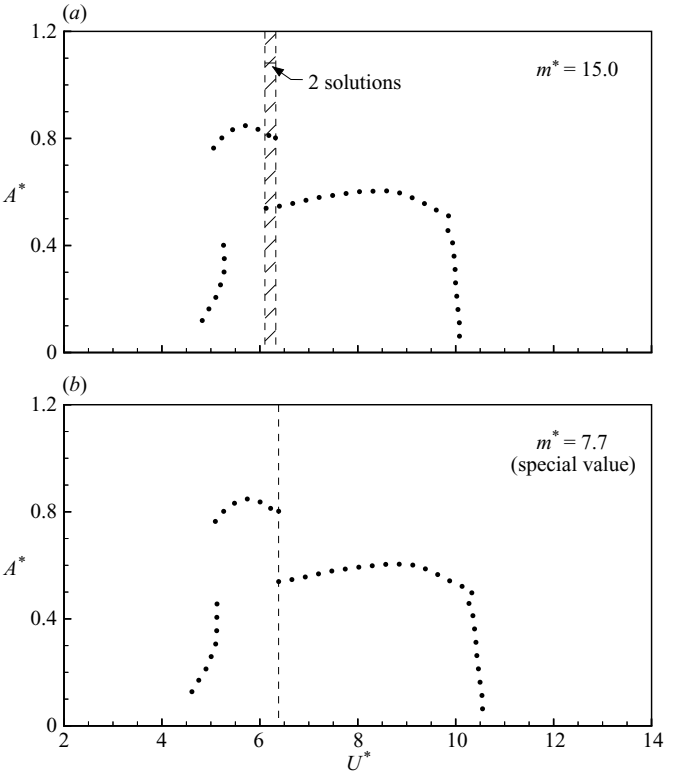

FIGURE 7. Predicted amplitude response for moderate mass ratio systems ($\zeta = 0$). (*a*) At $m^* = 15.0$ there is a small band of normalized velocity (U^*) in the upper to lower branch transition regions where two steady-state solutions exist. (*b*) As m^* is decreased to a special value of 7.7, there is no upper branch–lower branch overlap.

vortex-induced vibration cannot occur in these regions, in direct contradiction with published free vibration results.

In the transition region between the upper and lower branches, free vibration response is generally not precisely sinusoidal and exhibits variations in amplitude and frequency, as found by Govardhan & Williamson (2000). This would suggest that our controlled vibration force measurements (from purely sinusoidal motion) would not be easily applicable. However, even in this case, we shall apply, in an approximate manner, our quasi-steady model to determine the peak amplitudes.

In running the model, we encounter situations in which the solution may reside within the 2P–$2P_O$ overlap region. We then need to determine which mode of vortex formation the system takes on, as a function of time. On the basis of what one finds typically in free vibration experiments, we will assume that there is a 10 % chance, within each cycle of motion of the body, that the mode will switch between 2P and $2P_O$. Obviously, one has to make some assumption here, and it is clear that this is a somewhat arbitrary stipulation. However, it turns out from the model results that the value chosen for the probability of mode switch has very little influence on the response plot that we construct in figure 8(*b*). (For example, if we assume between 5 % and 30 % chance for a mode switch within each cycle, this would alter the resulting amplitude by typically less than 3 %.)

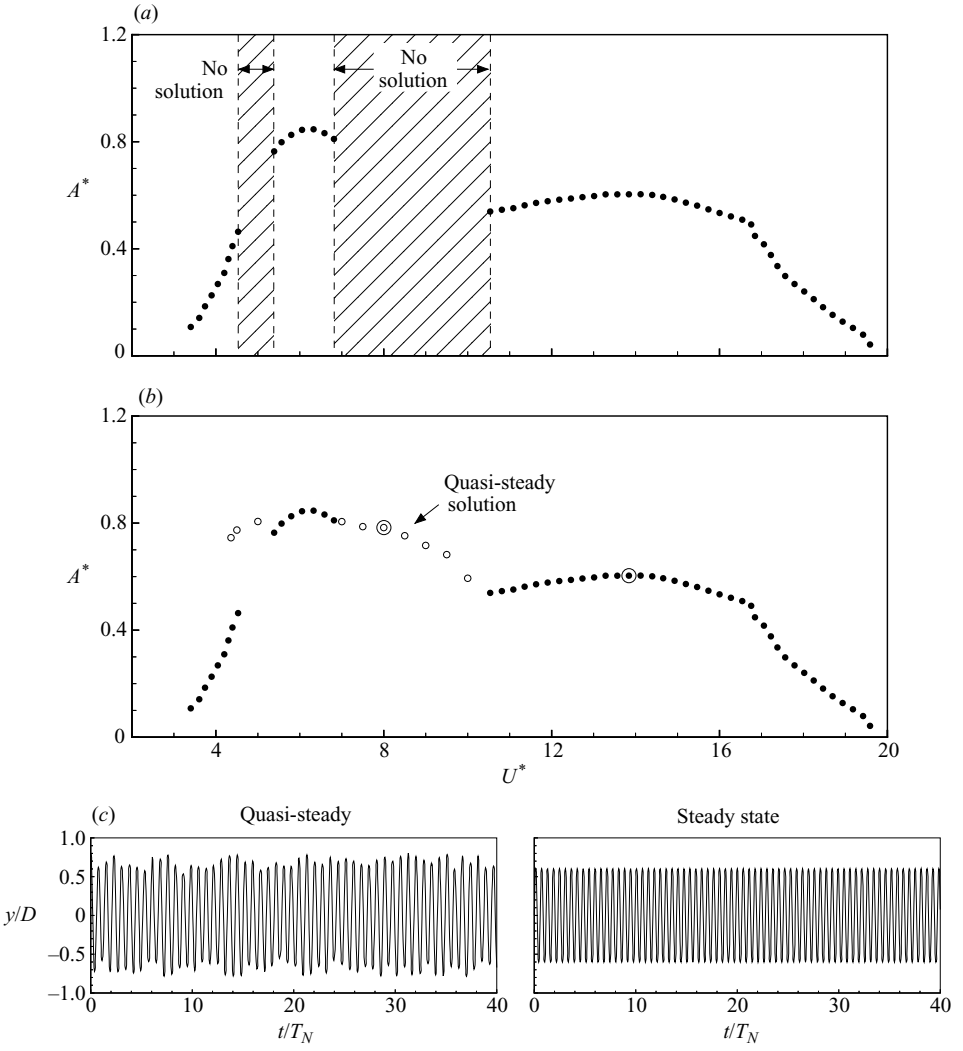

FIGURE 8. Predicted amplitude response character for a very low mass ratio system, $m^* = 1.0$ ($\zeta = 0$). (*a*) We find large gaps in the predicted response (●) where no steady-state solution exists. (*b*) We use our quasi-steady model to predict unsteady behaviour (○) in these gaps. (*c*) Predicted time traces for unsteady system dynamics (at location ◎) and for steady-state vibration (at location ⊙).

When we run our quasi-steady model, we find that the amplitude and frequency fluctuate as shown in figure 8(*c*). Computing the average amplitude of the top 10 % of the peaks, which is the parameter used by Hover *et al.* (1998) and Govardhan & Williamson (2006), we find that the predicted amplitude in this unsteady region fits well with the rest of our predicted response plot as shown in figure 8(*b*).

If we compare our complete predicted response plot (combining the steady-state solutions with the non-steady solutions) with directly measured free vibration response (for very low mass ratios around 1.0) from Govardhan & Williamson (2000), we find good qualitative agreement, both in the amplitude response and in the frequency response as shown in figure 9. We note that the slightly higher amplitudes of the

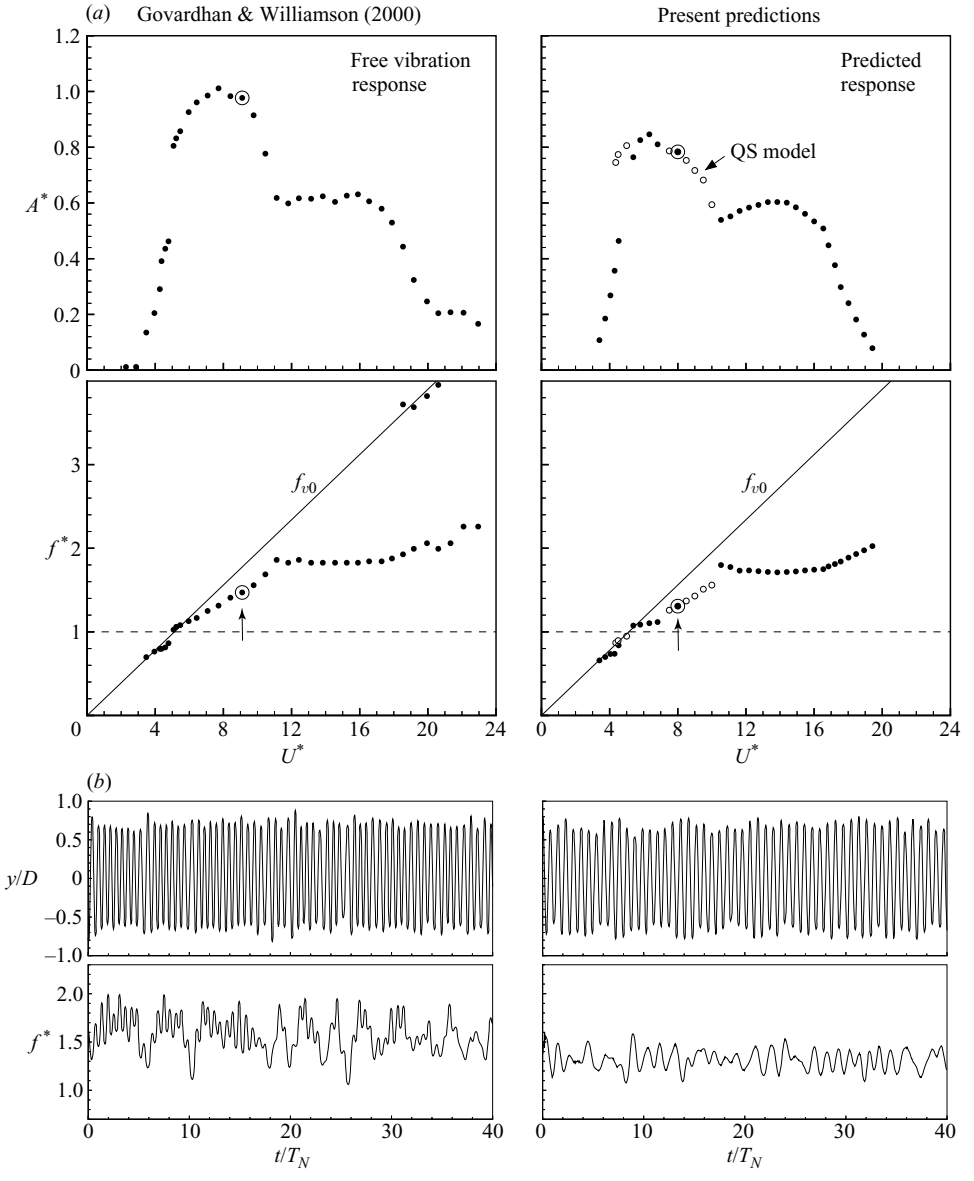

FIGURE 9. Comparison between measured free vibration amplitude and frequency response at $m^* = 1.19$ and predictions from controlled vibration at $m^* = 1.0$. We also show time traces (b) at selected locations (⊙) for each case. Measured free vibration response is from Govardhan & Williamson (2000).

upper branch from the free vibration experiments are due to the effects of the higher Reynolds number in this case, consistent with the results of Govardhan & Williamson (2006). In summary, the quasi-steady model appears to compare well with direct free vibration measurements. The model, employed at very low mass ratios, exhibits a regime of unsteady vibration, which contrasts with the character of intermittent mode jumps between bistable steady-state solutions associated with higher mass ratios.

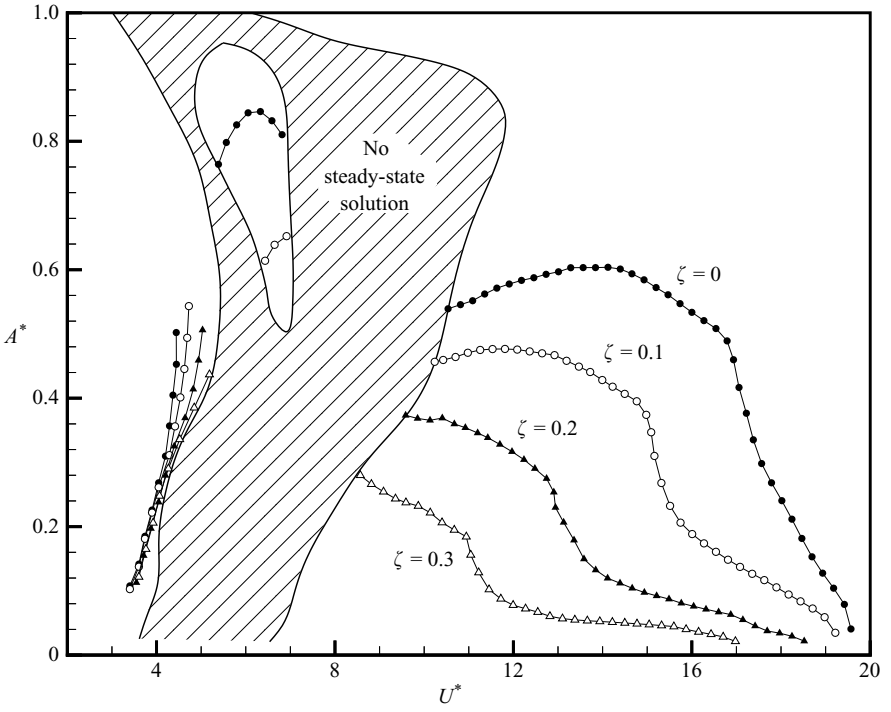

FIGURE 10. Map of steady and unsteady solutions in the A^*–U^* plane for $m^* = 1.0$. Where there is no steady-state solution, the system can only oscillate with unsteady vibration.

5.2. *Regime of unsteady response solutions in the A^*–U^* plane*

In the example described above, we focused on the case of a system at zero damping. If we consider higher values of the damping, we may define an entire region in the (U^*, A^*) plane where no steady-state solution is possible, as shown in figure 10, for $m^* = 1.0$. This map will be unique for each value of the mass ratio. The extent of the regime without steady solutions will grow as the mass ratio is reduced.

We may briefly explain how the 'void', where there exist no steady-state solutions, can occur. In the plot of amplitude versus wavelength (A^*–λ^*), mode regime boundaries are carefully defined from force measurements. A sketch of a representative boundary in figure 11(a) indicates that the value of C_{EA} jumps in value as it crosses the boundary, just as it does for the boundary between the 2S and 2P modes in figure 3(b). If, on the other hand, one now replots the boundary in the plane of amplitude versus normalized velocity (A^* versus U^*) then one must multiply all λ^* values (or U^*/f^* values) in figure 11(a) by the relevant normalized frequency (f^*) to construct the new plot in figure 11(b). (For a given mass ratio, m^*, (3.5) will yield this frequency, f^*). Our problem arises because the frequency (f^*) involves C_{EA}, and therefore has a jump change in value across the regime boundary. Thus, the regime boundary on the left for the 2S mode in figure 11(a) will get pulled to the left by the lower value of f^* on this side, while the 2P boundary in figure 11(a) gets pulled to the right by the higher value of f^*. In this way, a void appears between these two mode regimes, 2S and 2P in figure 11(b), where no steady-state solutions are found. As mass (m^*) becomes smaller so this difference in frequency (f^*) across the

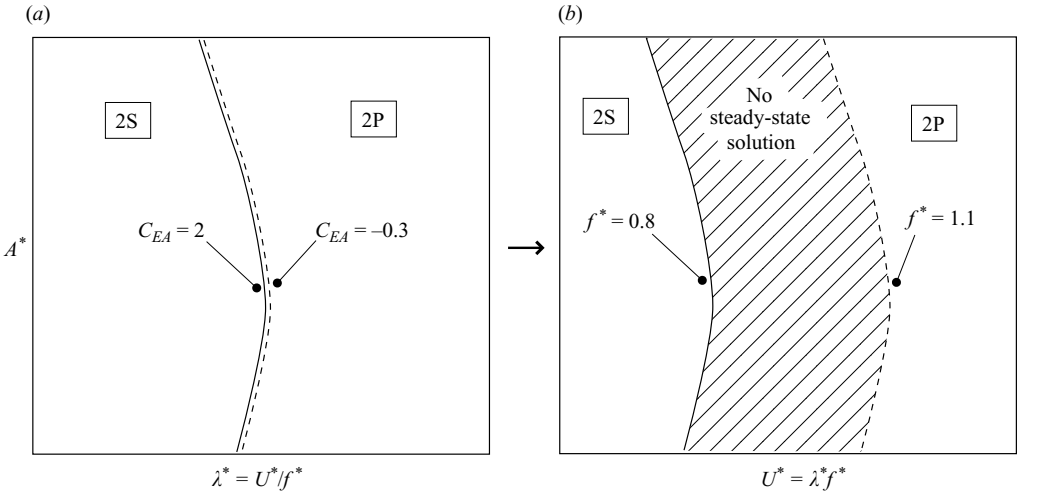

FIGURE 11. Schematic plot showing how a void with no steady-state solution occurs. The boundary between the 2S and 2P modes in the A^*–U^*/f^* plane (*a*) is stretched apart in the A^*–U^* plane (*b*) due to different values of C_{EA} (and thus different values of f^*) on opposite sides of the boundary. This leaves a void in the A^*–U^* plane where no steady-state solution occurs.

boundary gets larger, and the void grows, ultimately extending to infinite U^*, if the mass falls below a 'critical' value described in the next section.

5.3. *Frequency response at very low mass ratio*

We can also study the effect of very low mass ratio on the frequency response. For our brief discussion here, we focus on a system with zero damping. In the upper branch, the frequency ratio (f^*) is typically slightly higher than 1.0, as in figure 9. In the lower branch, the frequency is typically nearly constant over a wide range of normalized velocity; the value of this frequency increases, as mass ratio is diminished, as predicted from (3.5). The roughly constant value of f^* in the lower branch occurs because C_{EA} is nearly constant throughout the lower branch, as may be seen in the C_{EA} contours of figure 3. In between the upper and lower branches, only an unsteady vibration response exists for low mass ratio, and the frequency is found to increase approximately linearly with normalized velocity as we found in figure 9. The effect of mass ratio on the frequency response is found in figure 12, where one can immediately see the similar types of responses that we saw earlier in figure 9, except that the unsteady vibration regime grows dramatically as the mass is reduced to $m^* = 0.5$ and below.

At this point, we would like to describe what happens at very low mass ratios, $m^* < 1$. We first need to introduce the concept of a critical mass. From the frequency equation (3.5), we see that the effective added mass (C_{EA}) can play an important role in determining the frequency ratio ($f^* = f/f_N$). Govardhan & Williamson (2000) found that throughout the lower response branch in free vibration, the effective added mass was given approximately by $C_{EA} = -0.54$, so that the frequency ratio is given by

$$f^* = \sqrt{\frac{m^* + C_A}{m^* - 0.54}}. \tag{5.1}$$

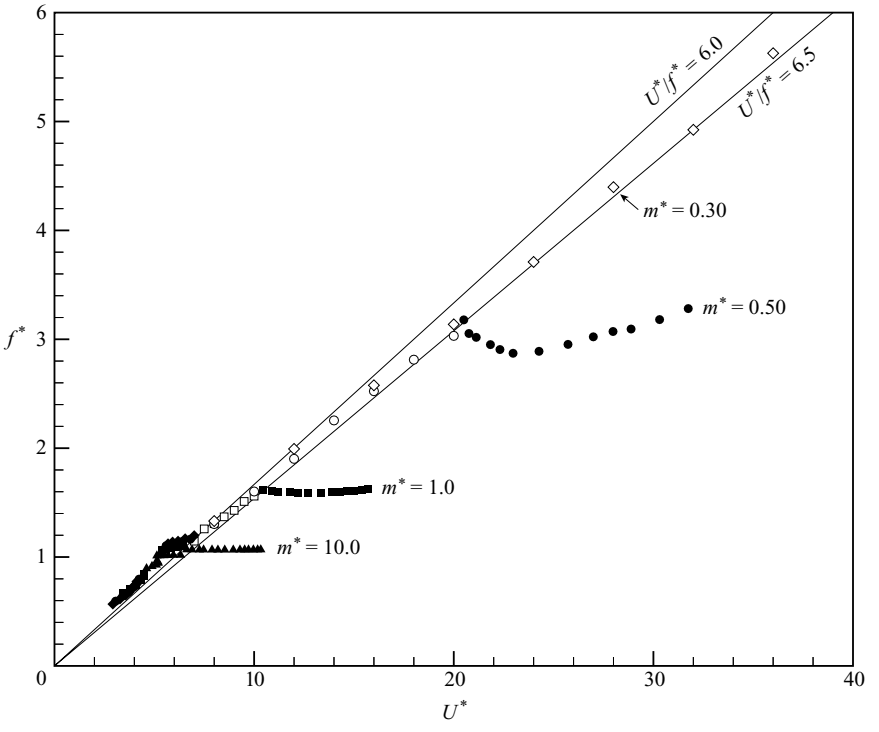

FIGURE 12. Predicted frequency response at different values of mass ratio. Solid symbols indicate steady-state behaviour and open symbols indicate unsteady behaviour. As mass ratio decreases, the range of normalized velocity (U^*) for the response becomes wider, extending to infinite values for $m^* < 0.36$.

Therefore, as the mass ratio (m^*) is reduced, the frequency ratio (f^*) in the lower branch can become large. Furthermore, when the mass ratio falls below a critical value of $m^*_{crit} = 0.54$, the lower branch will never be reached, and ceases to exist. The upper branch will then persist indefinitely, up to infinite normalized velocity ($U^* \to \infty$), giving an infinitely wide regime of resonances. In Morse & Williamson (2009*a*), we show the influence of Reynolds number on the value of the critical mass, and for $Re = 4000$, its value is $m^*_{crit} = 0.36$.

For extremely low mass, below the critical mass ratio, $m^* < 36\,\%$, the lower branch ceases to exist. In this case, the regime of large amplitude vibrations will extend from the end of the upper branch ($U^* \approx 7$) all the way to infinite normalized velocity. The example in figure 12, for $m^* = 0.30$, shows the unsteady vibration frequency response increasing throughout the range of plotted U^* at least up to 40, but in fact this trend will persist to infinite U^*, since $m^* < m^*_{crit}$ in this case.

The present quasi-steady model somewhat changes our interpretation of what happens when the mass ratio falls below the critical value (36 % in this case). Govardhan & Williamson (2000, 2002) described the critical mass phenomenon as involving an extension of the *upper branch* to infinite U^*. In fact, on the basis of the study here, we see that, rather than the upper branch extending to infinite U^*, it is the *unsteady vibration response* (which is a state *between* upper and lower branches) that is found to extend to infinite normalized velocity.

6. Conclusions

In this study, we have defined the fluid forces acting on a cylinder under controlled transverse vibration in a flow. Our high-resolution contour plots have been discussed before by Morse & Williamson (2009*b*,*c*), where extensive steady-state vibrations have been studied, along with the details of the vortex-formation modes. In this study, we also make use of the accurate determination of mode regime boundaries in the plane of amplitude–wavelength, which have been defined for the first time in such controlled vibration experiments. (Previous studies show a reasonably smooth variation of forces throughout the amplitude–wavelength plane.) The definition of the regime boundaries in our studies has enabled us, for the first time, not only to predict the general shape of amplitude response plots but also to show the existence of all the principal response branches found in free vibration experiments. However, the focus in this study is to develop a quasi-steady approach that can indicate what happens in cases of *transient or unsteady vibration.*

Cases of unsteady vibration arise when the response exhibits a transition between different response branches, which may seem like an unusual situation, but in fact it is quite common in free vibration systems, and is significant because *these unsteady vibrations represent the conditions giving the peak amplitude of response in low-mass systems.* In essence, we find that significant portions of the response plot, especially for the low mass ratios, are actually non-periodic. Such a regime in a response plot, which we refer to as a 'void', surprisingly does not admit steady-state solutions, although we know from free vibration that large vibrations can exist. The system cannot satisfy both the amplitude and frequency equations, defined in this study, at the same time. The key to understanding this phenomenon of a predicted 'void' is observing how the fluid forces make a distinct jump across the mode regime boundaries in the amplitude–wavelength plane. In an approximate manner, we attempt here to represent the system within these voids, using the quasi-steady model, and the resulting amplitude response predictions are surprisingly similar to what is found in high-amplitude free vibration experiments for very low mass ratios. The predicted response frequency variation is almost linearly increasing in the upper–lower branch transition, but becomes more constant when the response is firmly in the lower branch, which is also close to what is found in free vibration. For extremely low mass ratios, below a critical value ($m^* < 0.36$ in this case), the unsteady response regime stretches up to infinite normalized flow velocity, $U^* \to \infty$. In other words, the regime *without* the presence of steady-state solutions is the one that extends to infinite flow velocities, rather than the upper branch steady-state solutions, as supposed by Govardhan & Williamson (2002).

Our model can also represent the intermittent switching of modes, for higher mass ratios, that are found in free vibration. For moderate mass ratios (m^* of order 10), there exists a range of normalized velocities, U^*, for which there are two steady-state solutions to the equations of motion (corresponding to the upper and lower response branches). In this case, the response will switch intermittently between them depending on the vortex-formation mode selected by the flow (the 2P or $2P_O$ mode).

An unanswered question is what are the wake vortex dynamics in the transition region at low mass ratio? Of course, we do not expect that the entire wake is switching rapidly between a 2P and $2P_O$ vortex-formation mode. Lucor *et al.* (2005) found that the wake was quite three-dimensional in the upper to lower branch transition regions, in their case for $m^* = 2.0$. What seems plausible is that the wake shows different vortex dynamics at different points along the cylinder span in the transition region

yielding a net fluid forcing which is in between the forcing for the 2P and $2P_O$ modes. In contrast, for the intermittent switching behaviour at higher mass ratio, we suggest that the wake is largely two-dimensional for much of the time, when the response is seated for long periods on one branch or the other, between the intermittent mode switching.

The support from the Ocean Engineering Division of ONR, monitored by Dr. Tom Swean, is gratefully acknowledged (ONR contract N00014-04-1-0031 and N00014-07-1-0303). The authors would also like to thank Matt Horowitz for his extremely helpful and valuable input to this research.

REFERENCES

Bearman, P. W. 1984 Vortex shedding from oscillating bluff bodies. *Annu. Rev. Fluid Mech.* **16**, 195–222.

Bearman, P. W. & Branković, M. 2004 Experimental studies of passive control of vortex-induced vibration. *Eur. J. Mech.* B. *Fluids* **23**, 9–15.

Carberry, J., Sheridan, J. & Rockwell, D. 2005 Controlled oscillations of a cylinder: forces and wake modes. *J. Fluid Mech.* **538**, 31–89.

Gopalkrishnan, R. 1993 Vortex-induced forces on oscillating bluff cylinders. PhD thesis, MIT, Cambridge, MA, USA.

Govardhan, R. & Williamson, C. H. K. 2000 Modes of vortex formation and frequency response of a freely vibrating cylinder. *J. Fluid Mech.* **420**, 85–130.

Govardhan, R. & Williamson, C. H. K. 2002 Resonance forever: existence of a critical mass and an infinite regime of resonance in vortex-induced vibration. *J. Fluid Mech.* **473**, 147–166.

Govardhan, R. N. & Williamson, C. H. K. 2006 Defining the 'modified Griffin plot' in vortex-induced vibration: revealing the effect of Reynolds number using controlled damping. *J. Fluid Mech.* **561**, 147–180.

Hover, F. S., Davis, J. T. & Triantafyllou, M. S. 2004 Three-dimensionality of mode transition in vortex-induced vibrations of a circular cylinder. *Eur. J. Mech.* B. *Fluids* **23**, 29–40.

Hover, F. S., Techet, A. H. & Triantafyllou, M. S. 1998 Forces on oscillating uniform and tapered cylinders in crossflow. *J. Fluid Mech.* **363**, 97–114.

Khalak, A. & Williamson, C. H. K. 1996 Dynamics of a hydroelastic cylinder with very low mass and damping. *J. Fluids Struct.* **10**, 455–472.

Khalak, A. & Williamson, C. H. K. 1999 Motions, forces and mode transitions in vortex-induced vibrations at low mass-damping. *J. Fluids Struct.* **13**, 813–851.

Lucor, D., Foo, J. & Karniadakis, G. E. 2005 Vortex mode selection of a rigid cylinder subject to VIV at low mass-damping. *J. Fluids Struct.* **20**, 483–503.

Morse, T. L. & Williamson, C. H. K. 2009*a* The effect of Reynolds number on the critical mass phenomenon in vortex-induced vibration. *Phys. Fluids* **21**, 045105.

Morse, T. L. & Williamson, C. H. K. 2009*b* Fluid forcing, wake modes, and transitions for a cylinder undergoing controlled oscillation. *J. Fluids Struct.* **25**, 697–712.

Morse, T. L. & Williamson, C. H. K. 2009*c* Prediction of vortex-induced vibration response by employing controlled motion. *J. Fluid Mech.* **634**, 5–39.

Ongoren, A. & Rockwell, D. 1988 Flow structure from an oscillating cylinder. Part 2. Mode competition in the near wake. *J. Fluid Mech.* **191**, 225–245.

Parkinson, G. 1989 Phenomena and modelling of flow-induced vibrations of bluff bodies. *Progr. Aerospace Sci.* **26**, 169–224.

Ramberg, S. E. & Griffin, O. M. 1981 *Hydroelastic Response of Marine Cables and Risers*, pp. 1223–1245. Norwegian Institute of Technology.

Sarpkaya, T. 1977 Transverse oscillations of a circular cylinder in uniform flow. Part I. *Tech. Rep.* NPS-69SL77071. Nav. Postgrad. Sch., Monterey, CA, USA.

Sarpkaya, T. 1979 Vortex-induced oscillations. *Trans. ASME J. Appl. Mech.* **46**, 241–258.

Staubli, T. 1983 Calculation of the vibration of an elastically mounted cylinder using experimental data from forced vibration. *ASME J. Fluids Engng* **105**, 225–229.

Vikestad, K. 1998 Multi-frequency response of a cylinder subjected to vortex shedding and support motions. PhD thesis, Norwegian University of Science and Technology.

Williamson, C. H. K. & Govardhan, R. 2004 Vortex-induced vibrations. *Annu. Rev. Fluid Mech.* **36**, 413–455.

Williamson, C. H. K. & Roshko, A. 1988 Vortex formation in the wake of an oscillating cylinder. *J. Fluids Struct*. **2**, 355–381.